

- Restraint provided by exterior and core columns, which extended one floor above and below the modeled floor. The potential for large deflections and buckling of individual structural members and the floor system were included.

The results showed that:

- At lower elevated temperatures (approximately 100 °C to 400 °C), the floors thermally expanded and displaced the exterior columns outward by a few inches; horizontal displacement of the core columns was insignificant. None of the floors buckled as they thermally expanded, even with the exterior columns restrained so that no horizontal movement was allowed at the floors above and below the heated floor, which maximized column resistance to floor expansion. Even with this level of column restraint, the exterior columns did not develop a sufficient reaction force (push inward to resist the expansion outward) to buckle any of the floors.
- At higher elevated temperatures (above 400 °C), the floors began to sag as the floors' stiffness and strength were reduced with increasing temperature, and the difference in thermal expansion between the trusses and the concrete slab became larger. As the floor sagging increased, the outward displacement of the exterior columns was overcome, and the floors exerted an inward pull force on the exterior columns.
- Floor sagging was caused primarily by either buckling of truss web diagonals or disconnection of truss seats at the exterior wall or the core perimeter. Except for the truss seat failures near the southeast corner of the core in WTC 2 following the aircraft impact, web buckling or truss seat failure was caused primarily by elevated temperatures of the structural components.
- Analysis results from the detailed truss model found that the floors began to exert inward pull forces when floor sagging exceeded approximately 25 in. for the 60 ft floor span.
- Sagging at the floor edge was due to loss of vertical support at the truss seats. The loss of vertical support was caused in most cases by the reduction in vertical shear capacity of the truss seats due to elevated steel temperatures.
- Case B impact damage and thermal loads for WTC 1 floors resulted in floor sagging on the south side of the tower over floors that reasonably matched the location of inward bowing observed on the south face. Case A impact damage and thermal loads did not result in sagging on the south side of the floors.
- Cases C and D impact damage and thermal loads for WTC 2 both resulted in floor sagging on the east side of the tower over floors that reasonably matched the location of inward bowing observed on the east face. However, Case D provided a better match.

Exterior Wall

Exterior wall models were developed for the south face of WTC 1 (floors 89 to 106) and the east face of WTC 2 (floors 73 to 90). These sections were selected based on photographic evidence of column bowing.

Many of the simulation conditions were similar to those for the isolated core modeling: removal of aircraft-damaged structural components, representation of lower floors by springs, temperature-varying steel properties, gravity loads applied at each floor, post-impact column forces applied at the 106th floor, and temperature histories applied at 10 min intervals with linear ramping between time intervals.

The analysis results showed that:

- Inward pull forces were required to produce inward bowing consistent with the displacements measured from photographs. The inward pull was caused by sagging of the floors. Heating of the inside faces of the exterior columns also contributed to inward bowing.
- Exterior wall sections bowed outward in a pushdown analysis when several consecutive floors were disconnected, the interior face of the columns was heated, and column gravity loads increased (e.g., due to load redistribution from the core and hat truss). At lower temperatures, thermal expansion of the inside face was insufficient to result in inward bowing of the entire exterior column. At higher temperatures, outward bowing resulted from the combined effects of reduced steel strength on the heated inside face, which shortened first under column gravity loads, and the lack of lateral restraint from the floors.
- The observed inward bowing of the exterior wall indicated that most of the floor connections must have been intact to cause the observed bowing.
- The extent of floor sagging observed at each floor was greater than that predicted by the full floor models. The estimates of the extent of sagging at each floor was governed by the combined effects of insulation damage and fire; insulation damage estimates were limited to areas subject to direct debris impact. Other sources of floor and insulation damage from the aircraft impact and fires (e.g., insulation damage due to shock and subsequent vibrations as a result of aircraft impact or concrete slab cracking and spalling as a result of thermal effects) were not included in the floor models.
- Case B impact damage and thermal loads for the WTC 1 south wall, combined with pull-in forces from floor sagging, resulted in an inward bowing of the south face that reasonably matched the observed bowing. The lack of floor sagging for the Case A impact damage and thermal loads resulted in no inward bowing for the south face.
- Cases D impact damage and thermal loads for the WTC 2 east wall, combined with pull-in forces from floor sagging, resulted in an inward bowing of the east face that reasonably matched the observed bowing.

Phase 3: Global Modeling

The global models were used for the two final simulations and provided complete analysis of results and insight into the subsystem interactions leading to the probable collapse sequence. Based upon the results of the major subsystem analyses, impact damage and thermal loads for Cases B and D were used for WTC 1 and WTC 2, respectively. The models extended from floor 91 for WTC 1 and floor 77 for WTC 2 to the roof level in both towers. Although the renditions of the structural components had been reduced in complexity while maintaining essential nonlinear behaviors, based on the findings from the component and subsystem modeling, the global models included many of the features of the subsystem models:

- Removal of aircraft-damaged structural components.
- Application of gravity loads following removal of aircraft damaged components and prior to thermal loading.
- Temperature-dependent concrete and steel properties.
- Creep strains for column components.
- Representation of lower floors by springs.
- Local temperature histories applied at 10 min intervals with linear ramping between time intervals.

There were several adjustments to the models based on the findings from the subsystem modeling:

- Removal of thermal expansion from the spandrels and equivalent slabs in the tenant area to avoid local buckling that affected convergence but had little influence on global collapse initiation.
- Representing the WTC 2 structure above the 86th floor as a single “super-element” to reduce model complexity. The floors above the impact zone had only exhibited linear behavior in the previous analyses. This modification assumed linear behavior of the hat truss, which was checked as part of the review of analysis results.
- Representation of the lower part of the tower (starting several floors below the impact damage) as a super-element. This prevented the use of construction sequence in applying gravity loads to the model (where loads are applied in stages to simulate the construction of the building). The lack of construction sequence increased the forces on the exterior columns slightly, and decreased those on the core columns slightly.

The inclusions of creep for column components was necessary for the accuracy of the models, but its addition also greatly increased the computation time. As a result, the simulations of WTC 1 took 22 days and those of WTC 2 took 14 days on a high-end computer workstation. The results of these simulations are presented in Section 6.14.

6.7 THE AIRCRAFT STRUCTURAL MODEL

Due to their similarity, the two Boeing 767-200ER aircraft were represented by a single, finite element model, two views of which are shown in Figure 6-13. The model consisted of about 800,000 elements. The typical element dimensions were between 1 in. and 2 in. for small components, such as spar or rib flanges, and 3 in. to 4 in. for large parts such as the wing or fuselage skin. Structural data on which to base the model were collected from the open literature, electronic surface models and CAD drawings, an inspection of a 767-300ER, Pratt and Whitney Engine Reference Manuals, American Airlines and United Airlines, and the Boeing Company website.

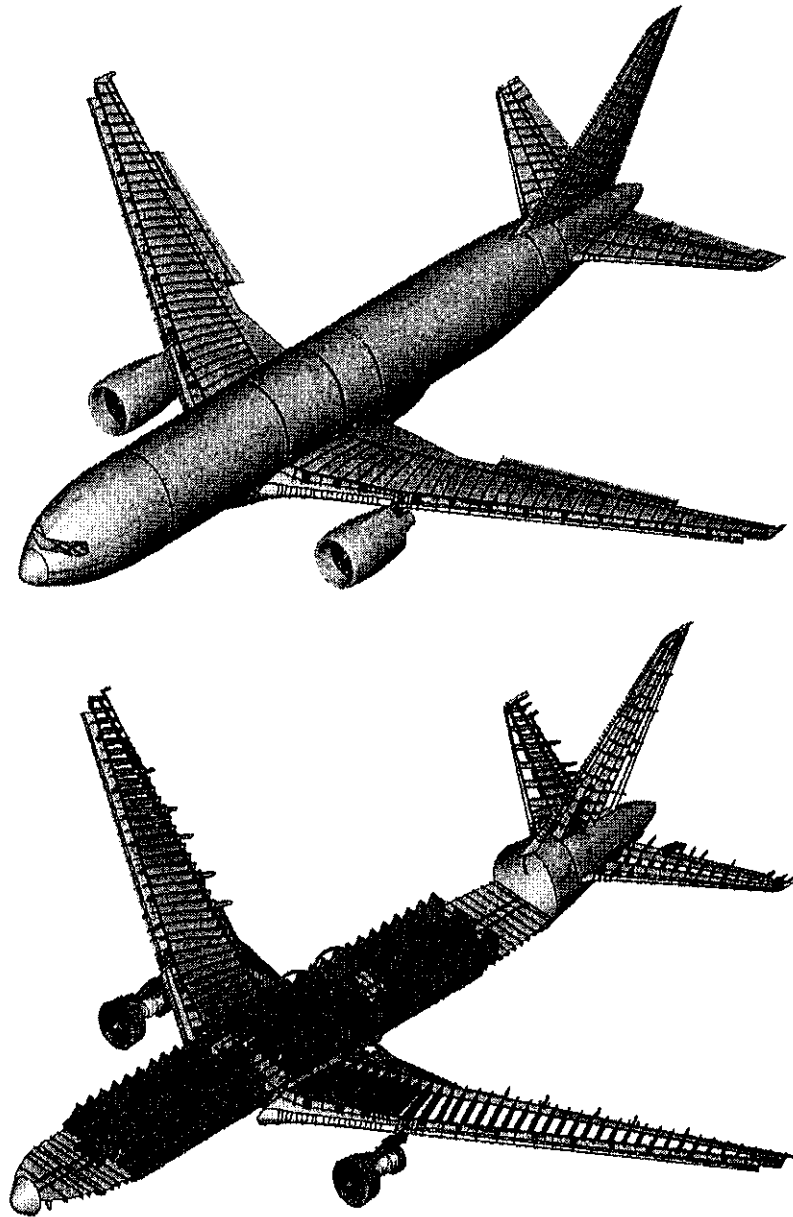


Figure 6-13. Finite element model of the Boeing 767-200ER.

More detailed models of subsections of the aircraft were constructed for the component level analyses described below. Special emphasis was placed on modeling the aircraft engines, due to their potential to produce significant damage to the tower components. The element dimensions were generally between 1 in. and 2 in., although even smaller dimensions were required to capture some details of the engine geometry. The various components of the resulting engine model are shown in Figure 6–14. Fuel was distributed in the wing as shown in Figure 6–15 based on a detailed analysis of the fuel distribution at the time of impact.

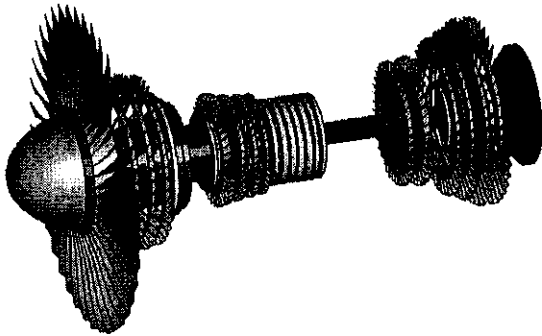


Figure 6–14. Pratt & Whitney PW4000 turbofan engine model.

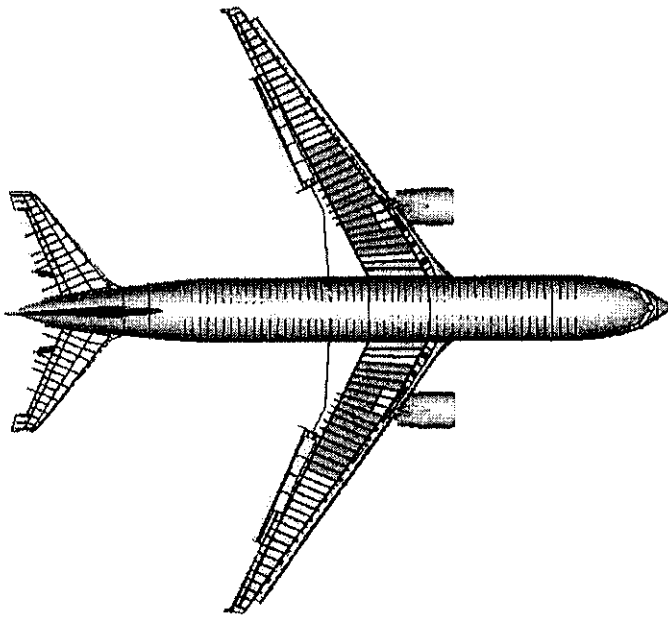


Figure 6–15. Boeing 767-200ER showing the jet fuel distribution at time of impact.

6.8 AIRCRAFT IMPACT MODELING

6.8.1 Component Level Analyses

Prior to conducting the full simulations of the aircraft impacting the towers, a series of smaller scale simulations was performed to develop understanding of how the aircraft and tower components fragmented and to develop the simulation techniques required for the final computations. These simulations began with finely meshed models of key components of the tower and aircraft structures and progressed to relatively coarsely meshed representations that could be used in the global models. Examples of these component-level analyses included impact of a segment of an aircraft wing with an exterior column, impact of an aircraft engine with exterior wall panels, and impact of a fuel-filled wing segment with exterior wall panels.

Figure 6–16 shows two frames from the last of these analyses, with the wing segment entering from the left, being fragmented as it penetrates the exterior columns, and spraying jet fuel downstream.

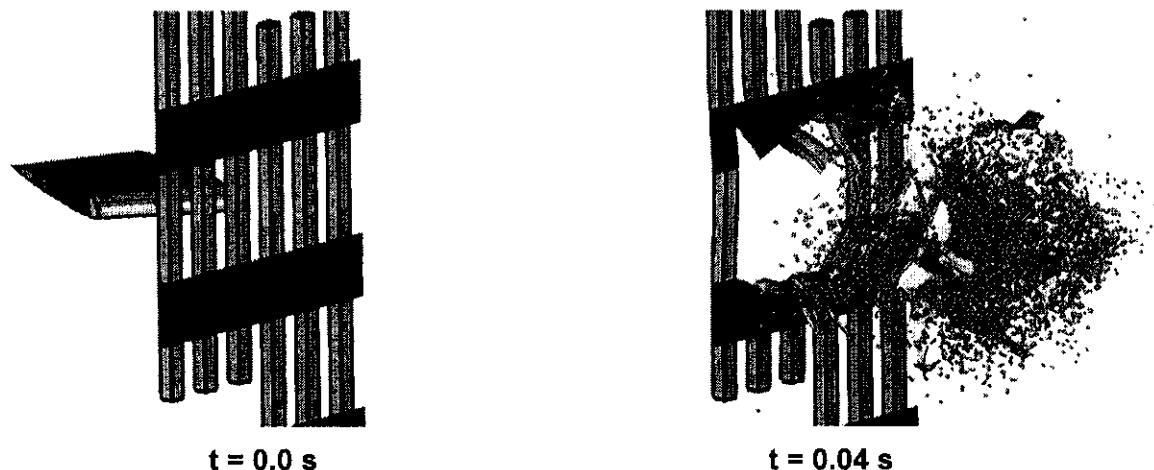


Figure 6–16. Calculated impact on an exterior wall by a fuel-laden wing section.

The Investigation Team gained valuable knowledge from these component impact analyses, for example:

- Moving at 500 mph, an engine broke any exterior column it hit. If the engine missed the floor slab, the majority of the engine core remained intact and had enough residual momentum to sever a core column upon direct impact.
- The impact of the inner half of an empty wing significantly damaged exterior columns but did not result in their complete failure. Impact of the same wing section, but filled with fuel, did result in failure of the exterior columns.

6.8.2 Subassembly Impact Analyses

Next, a series of simulations were performed for intermediate-sized sections of a tower. These subassembly analyses investigated different modeling techniques and associated model sizes, run times, numerical stability, and impact response. Six simulations were performed of an aircraft engine impacting a subassembly that included structural components from the impact zone on the north face of WTC 1, exterior panels, truss floor structures, core framing, and interior contents (workstations). One response of the structure to the engine impact is shown in Figure 6–17.

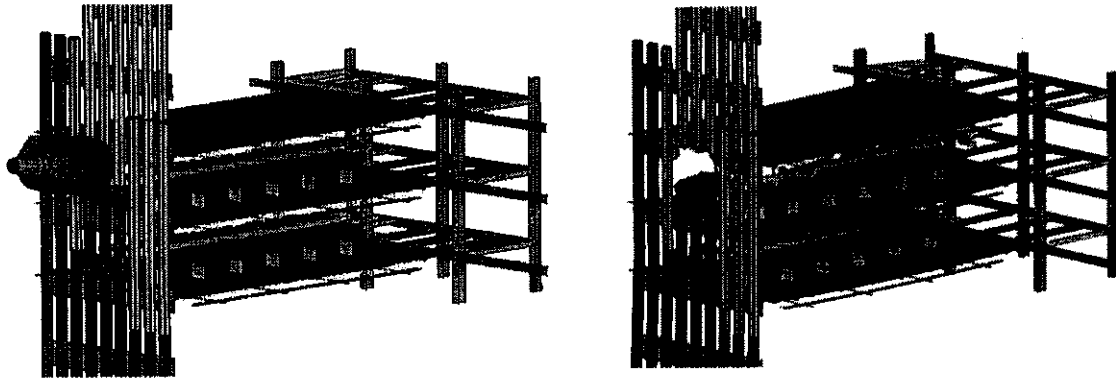


Figure 6–17. Response of a tower subassembly model to engine impact.

Typical knowledge gained from these simulations were:

- The mass of the concrete floor slab and nonstructural contents had a greater effect on the engine deceleration and subsequent damage than did the concrete strength.
- Variation of the failure criteria of the welds in the exterior columns did not result in any noticeable difference in the damage pattern or the energy absorbed by the exterior panels.

6.8.3 Aircraft Impact Conditions

From the NIST photographic and video collection, the speed and orientation of the aircraft (Table 6–4) were estimated at the time of impact. The geometry of the wings, different in flight from that at rest, was estimated from the impact pattern in the photographs and the damage documented on the exterior panels by NIST. United Airlines and American Airlines provided information on the contents of the aircraft, the mass of jet fuel, and the location of the fuel within the wing tanks.

Table 6–4. Summary of aircraft impact conditions.

Condition	AA 11 (WTC 1)	UAL 175 (WTC 2)
Impact Speed (mph)	443 ± 30	542 ± 24
Vertical Approach Angle	10.6° ± 3° below horizontal (heading downward)	6° ± 2° below horizontal (heading downward)
Lateral Approach Angle	180.3° ± 4° clockwise from Plan North ^a	13° ± 2° clockwise from Plan North ^a
Roll Angle (left wing downward)	25° ± 2°	38° ± 2°

a. Plan North is approximately 29 degrees clockwise from True North.

6.8.4 Global Impact Analysis

From the component and subassembly simulations, it became apparent that each computation of the full tower and aircraft would take weeks. Furthermore, the magnitude and location of damage to the tower structure were sensitive to a large number of initial conditions, to assumptions in the representation of the collision physics, and to any approximations in the numerical methods used to solve the physics equations. Thus, it was necessary to choose a manageable list of the factors that most influenced the outcome of a simulation. Careful screening was conducted at the component and subassembly levels, leading to identification of the following prime factors:

- Impact speed,
- Vertical approach angle of the aircraft,
- Lateral approach angle of the aircraft,
- Total aircraft weight,
- Aircraft materials failure strain,
- Tower materials failure strain, and
- Building contents weight and strength.

Guided by these results and several preliminary global simulations, two global simulations were selected for inclusion in the four-step simulation of the response of each tower, as described in Section 6.1. The conditions for these four runs are shown in Table 6–5. The computers simulate the aircraft flying into the tower, calculated the fragments that were formed from both the aircraft and the building itself, and then followed the fragments. The jet fuel, atomized upon impact into about 60,000 “blobs” averaging one pound, dispersed within and outside the building. Each simulation continued until the debris motion had reduced to a level that was not expected to produce any significant further impact damage.

Table 6–5. Input parameters for global impact analyses.

Analysis Parameters		WTC 1		WTC 2	
		Case A	Case B	Case C	Case D
Flight Parameters	Impact Speed	443 mph	472 mph	542 mph	570 mph
	Vertical Approach Angle	10.6°	7.6°	6.0°	5.0°
	Lateral Approach Angle	180.0°	180.0°	13.0°	13.0°
Aircraft Parameters	Weight	100 %	105 %	100 %	105 %
	Failure Strain	100 %	125 %	100 %	115 %
Tower Parameters	Failure Strain	100 %	80 %	100 %	90 %
	Live Load Weight ^a	25 %	20 %	25 %	20 %
	Contents Strength	100 %	100 %	100 %	80 %

a. Live load weight expressed as a percentage of the design live load.

These simulations each took about 2 weeks on a 12-node computer cluster. Figure 6–18 shows six frames from the animation of one such simulation.

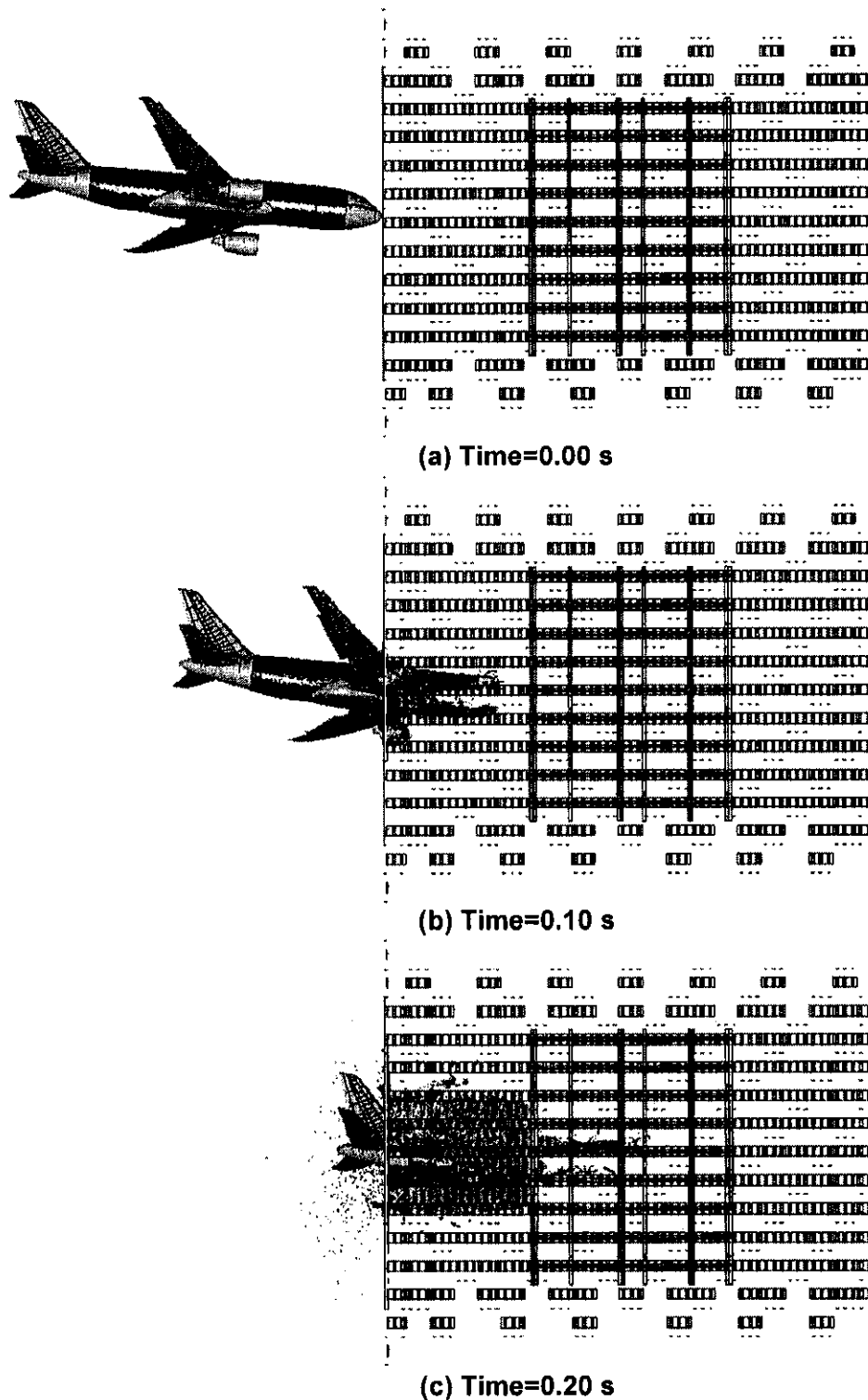
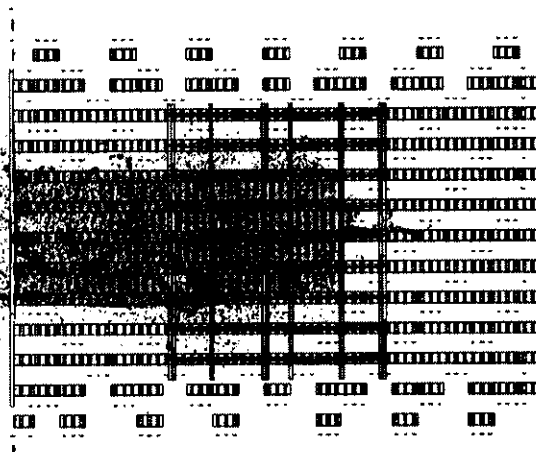
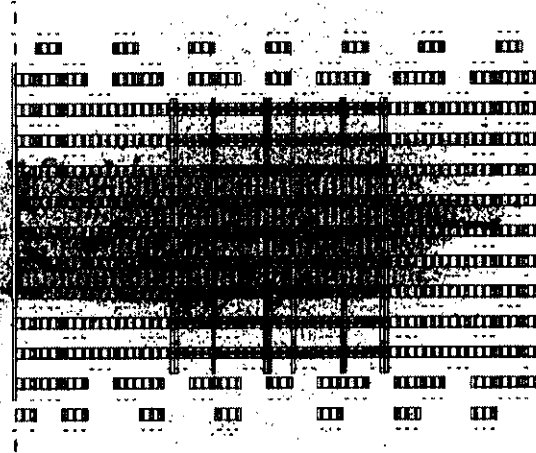


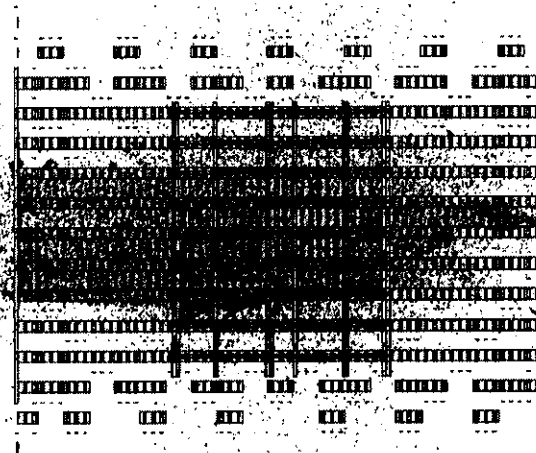
Figure 6–18. Side view of simulated aircraft impact into WTC 1, Case B.



(d) Time=0.30 s



(e) Time=0.40 s



(f) Time=0.50 s

Figure 6-18. Side view of simulated aircraft impact into WTC 1, Case B (Cont.)

6.9 AIRCRAFT IMPACT DAMAGE ESTIMATES

6.9.1 Structural and Contents Damage

Each of the four global simulations generated information about the state of the structural components following the impact of the aircraft. The four degrees of column damage are defined as follows and shown graphically in Figure 6–19. The unstrained areas are blue and the highly strained areas are red.

- Lightly damaged column: column impacted, but without significant structural deformation;
- Moderately damaged column: visible local distortion, but no deformation of the column centerline;
- Heavily damaged column: Permanent deflection of the column centerline; and
- Failed column: Column severed.

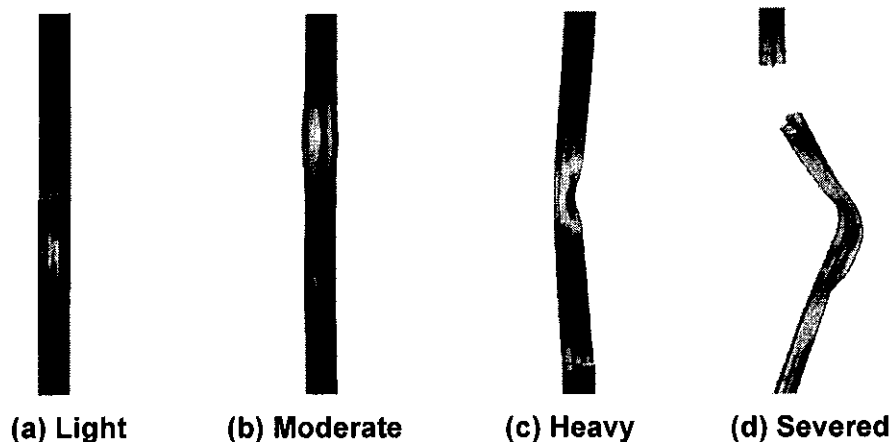


Figure 6–19. Column damage levels.

Figure 6–20 shows the calculated damage to a floor slab. Figure 6–21 shows the response of the furnishings and the jet fuel to the impact. Figures 6–22 through 6–25 show the combined damage for all floors for the four global simulations. The latter proved useful in visualizing the extent of aircraft impact in one graphic image.

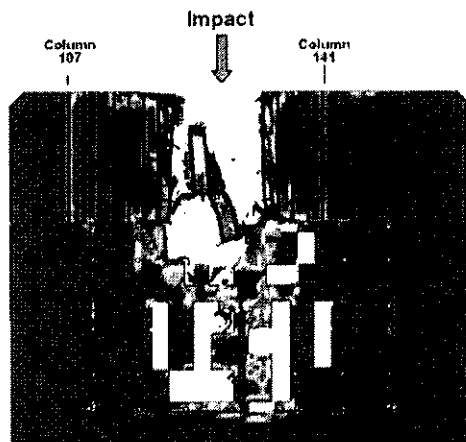
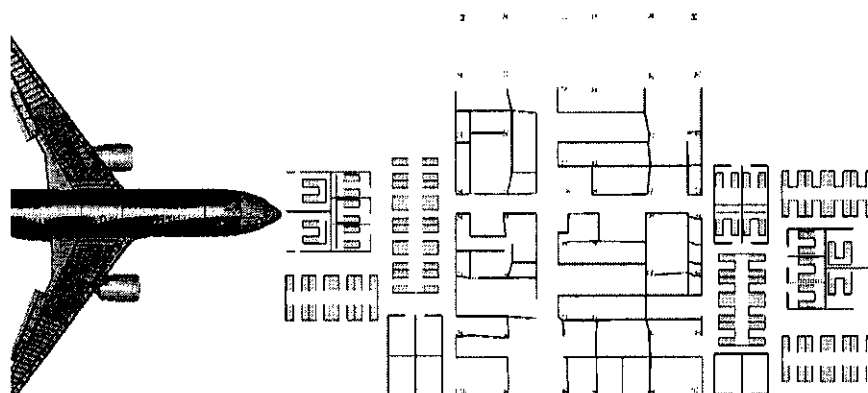
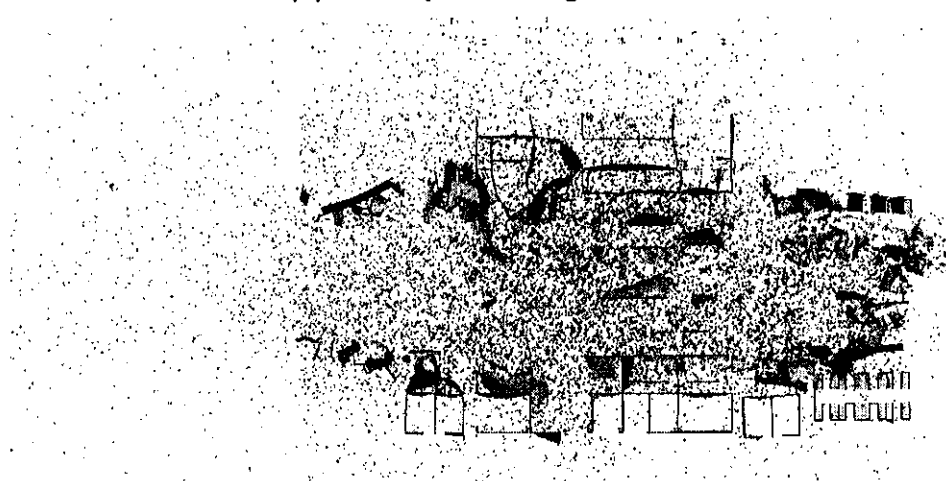


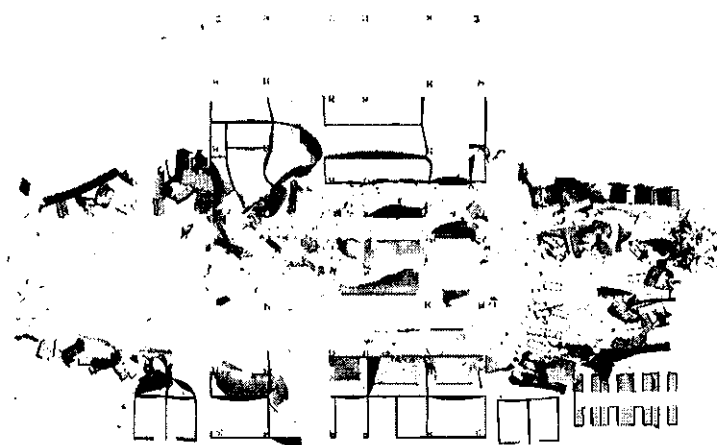
Figure 6–20. Case B damage to the slab of floor 96 of WTC 1.



(a) Pre-impact configuration



(b) Calculated impact response



(c) Calculated impact response (fuel removed)

Figure 6–21. Case B simulation of response of contents of 96th floor of WTC 1.



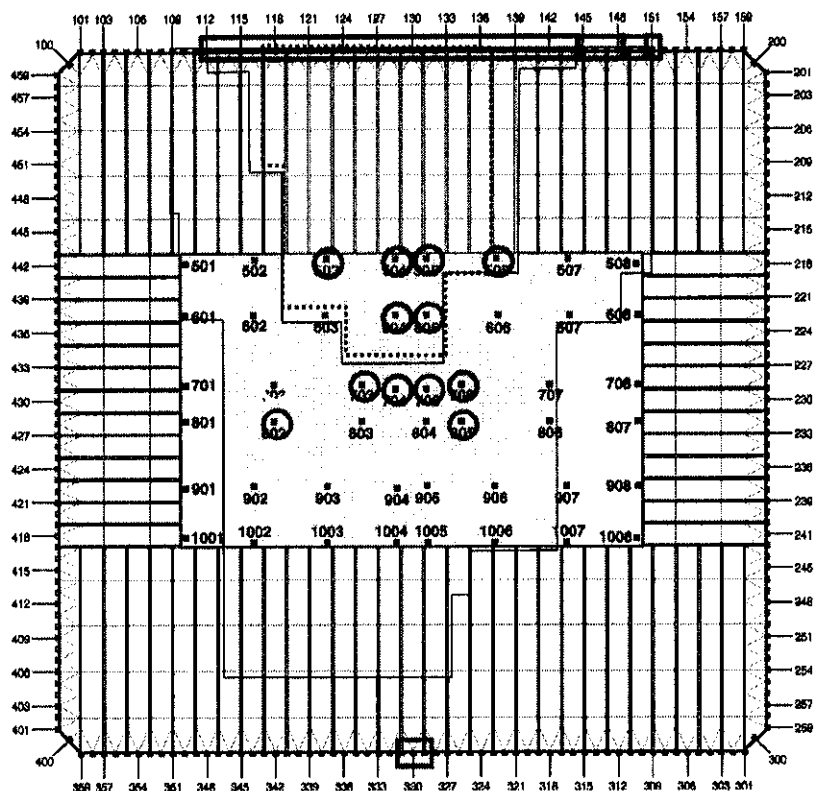
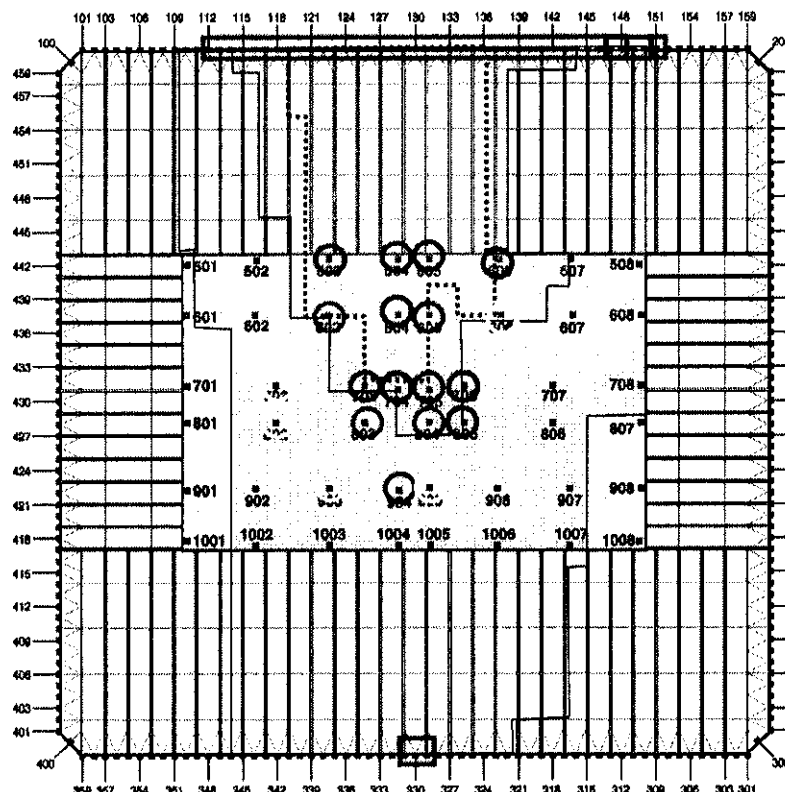
Severe Floor DamageFloor fireproofing Floor system structural damage Floor system removed **Column Damage**Severed Heavy damage Moderate damage Light damage 

Figure 6-22. Combined structural damage to the floors and columns of WTC 1, Case A.

Figure 6-23. Combined structural damage to the floors and columns of WTC 1, Case B.



Severe Floor Damage

Floor fireproofing ☐

Floor system structural damage ☐

Floor system removed ☐

Column Damage

Severed ☐

Heavy damage ☐

Moderate damage ☐

Light damage ☐

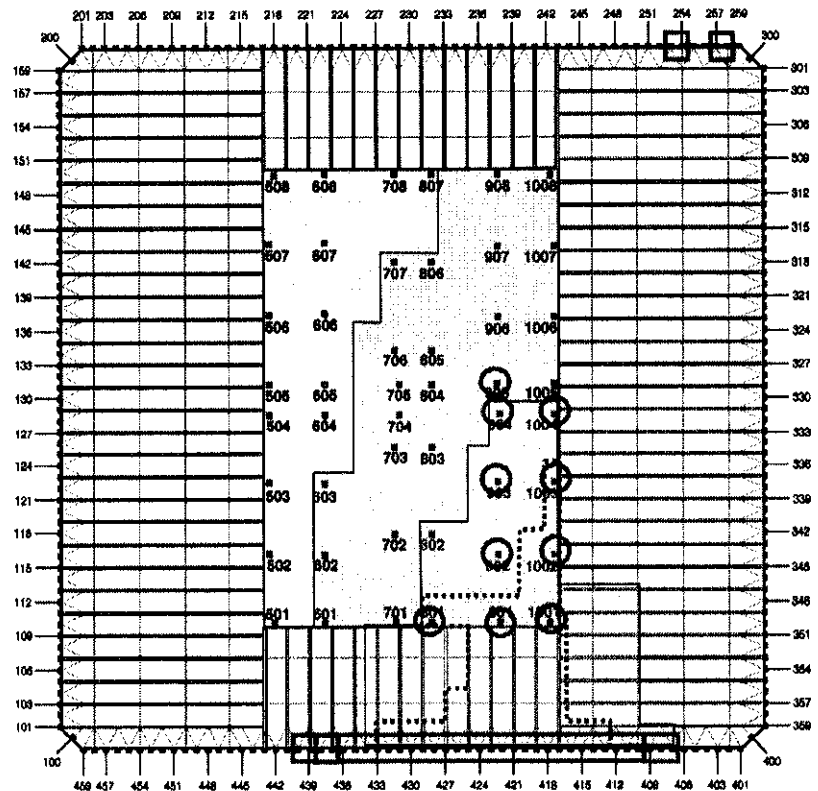
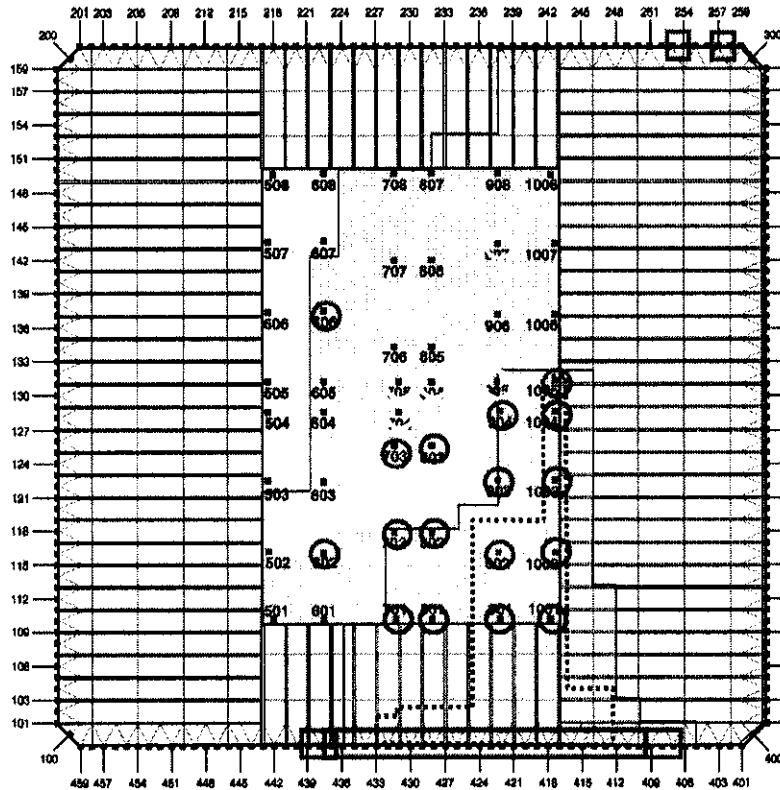


Figure 6-24. Combined structural damage to the floors and columns of WTC 2, Case C.

Figure 6-25. Combined structural damage to the floors and columns of WTC 2, Case D.



6.9.2 Validity of Impact Simulations

Assessment of the aircraft impact simulations of exterior damage to the towers involved comparing the predicted perimeter wall damage near the impact zone with post-impact photographs of the walls. Figure 6–26 shows a photograph of the north face of WTC 1 after impact and the results of the Case A simulation. The calculated silhouettes capture both the position and shape of the actual damage.

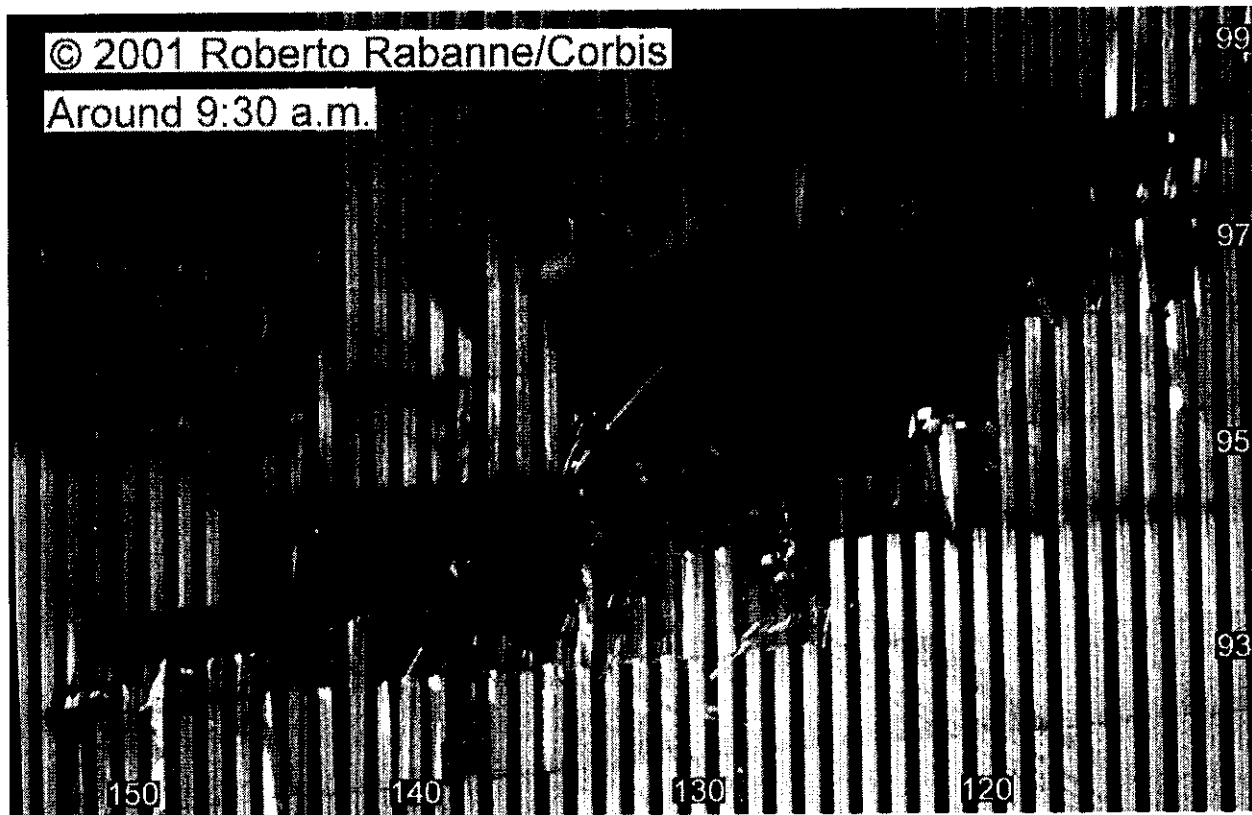
Figures 6–27 and 6–28 depict more detailed comparisons between the observed and calculated damage. The aircraft hole is shown in white. The colored dots characterize the mode in which the steel or connection failed (e.g., severed bolt, ripped weld) and the magnitude of the deformation of the steel:

- Green: proper match of failure mode and magnitude
- Yellow: proper match in the failure mode, but not the magnitude
- Red: neither the failure mode nor the magnitude matched
- Black: the observed damage was obscured by smoke, fire, or other factors

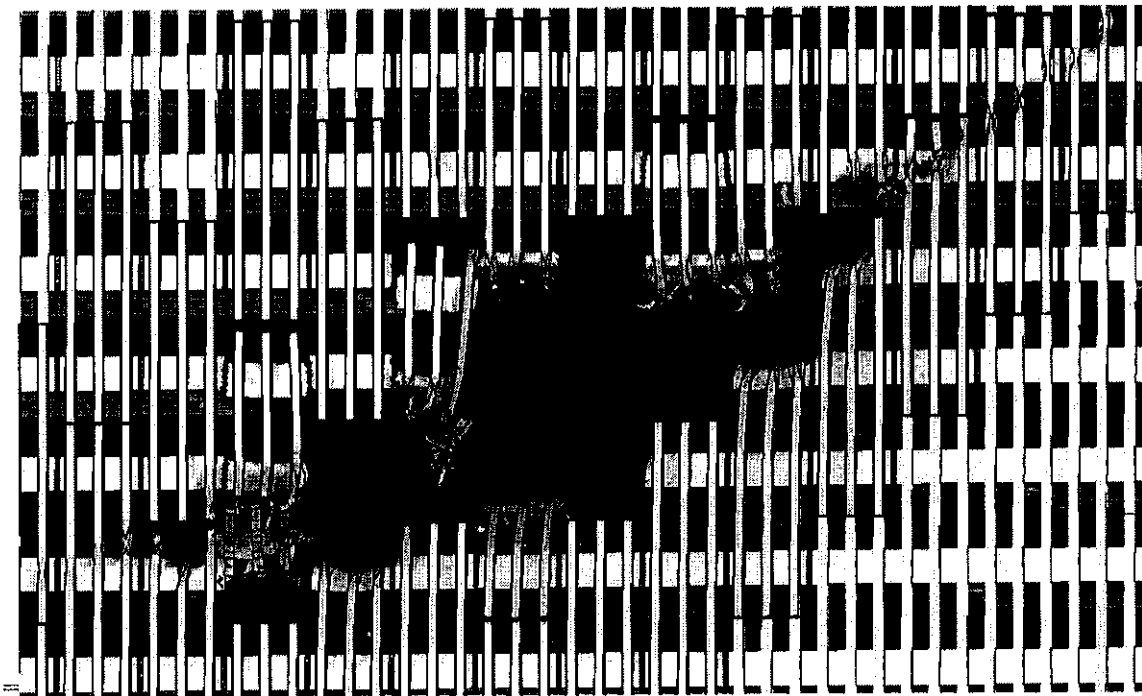
The predominance of green dots and the scarcity of red dots indicate that the overall agreement with the observed damage was very good. The agreement for Cases B and D was slightly lower.

Assessment of the accuracy of the predictions of damage inside the buildings was more difficult, as NIST could not locate any interior photographs near the impact zones. Three comparisons were made:

- The Case A simulation for WTC 1 predicted that the walls of all three stairwells would have been collapsed. This agreed with the observations of the building occupants. The Case A simulation for WTC 2 showed that the walls of stairwell B would have been damaged, but that Stairwell A would have been unaffected. Stairwell C was not included in the WTC 2 model, but is adjacent to where damage occurred. The building occupants reported that Stairwells B and C were impassable; Stairwell A was damaged but passable.
- The two simulations of WTC 2 showed accumulations of furnishings and debris in the northeast corner of the 80th and 81st floors. These piles were observed in photographs and videos.
- Two pieces of landing gear penetrated WTC 1 and landed to the south of the tower. The Case B prediction showed landing gear penetrating the building core, but stopping before reaching the south exterior wall. For WTC 2, a landing gear fragment and the starboard engine penetrated the building and landed to the south. The Case D prediction correctly showed the main landing gear emerging from the northeast corner of WTC 2. However, Case D showed that engine not quite penetrating the building. Minor modifications to the model (all within the uncertainty of the input data) would have resulted in the engine passing through the north exterior wall of the tower.



(a) Observed Damage



(b) Calculated damage

Figure 6-26. Observed and Case A calculated damage to the north face of WTC 1.

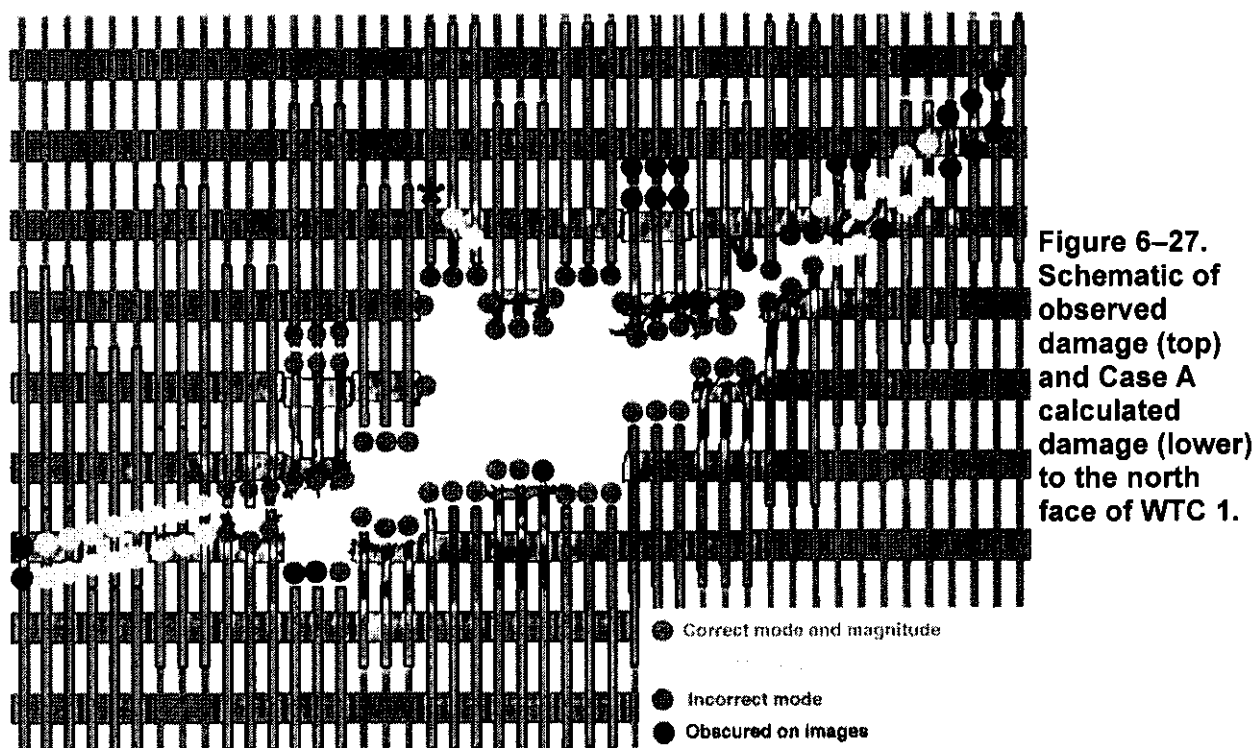
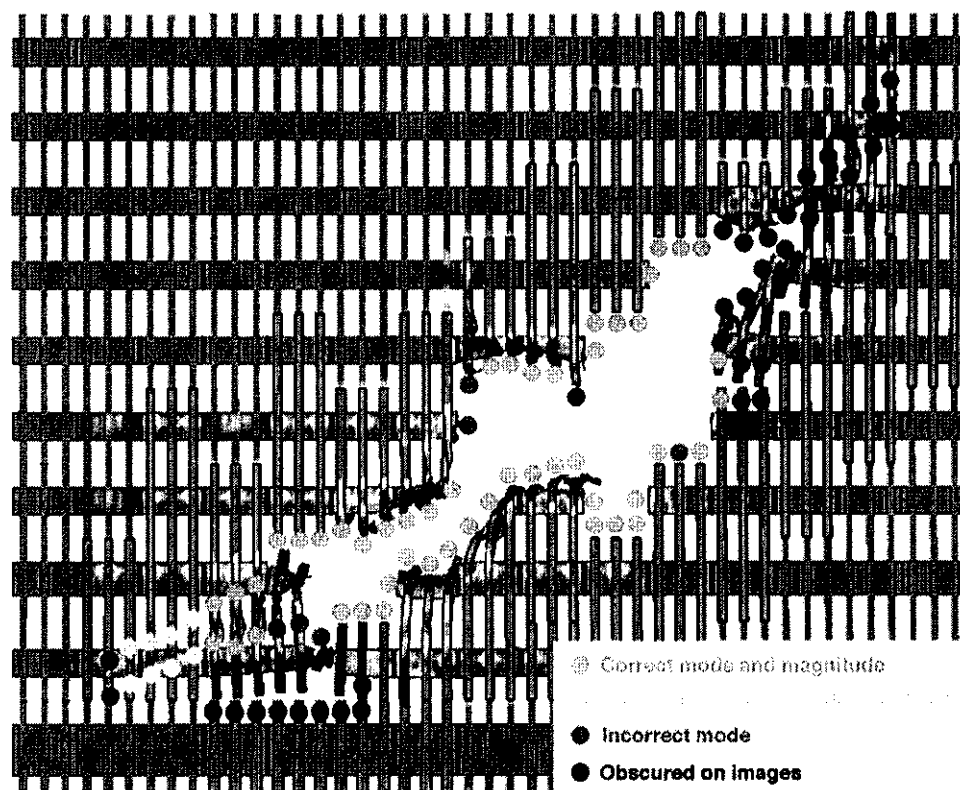


Figure 6-28. Schematic of observed damage (above) and Case C calculated damage (right) to the south face of WTC 2.



Not all of the observables were closely matched by the simulations due to the uncertainties in exact impact conditions, the imperfect knowledge of the interior tower contents, the chaotic behavior of the aircraft breakup and subsequent debris motion, and the limitations of the models. In general, however, the results of the simulations matched these observables sufficiently well that the Investigation Team could rely on the predicted trends.

Simulations of the damage to the core columns had been performed previously by staff of Weidlinger Associates, Inc. (WAI) and the Massachusetts Institute of Technology (MIT). Each developed a range of numbers of failed and damaged columns, as did NIST. The range of the MIT results straddled the NIST results. WAI's analysis resulted in more failed and damaged columns, with WTC 2 being unstable immediately following impact.

6.9.3 Damage to Thermal Insulation

The dislodgement of thermal insulation from structural members could have occurred as a result of (a) direct impact by debris and (b) inertial forces due to vibration of structural members as a result of the aircraft impact. The debris from the aircraft impact included the fragments that were formed from both the aircraft (including the contents and fuel) and the building (structural members, walls, and furnishings). In interpreting the output of the aircraft impact simulations, NIST assumed that the debris impact dislodged insulation if the debris force was strong enough to break a gypsum board partition immediately in front of the structural component. Experiments at NIST confirmed that an array of 0.3 in. diameter pellets traveling at approximately 350 mph stripped the insulation from steel bars like those used in the WTC trusses.

Determining the adherence of SFRM outside the debris zones was more difficult. There was photographic evidence that some fraction of the SFRM was dislodged from perimeter columns not directly impacted by debris.

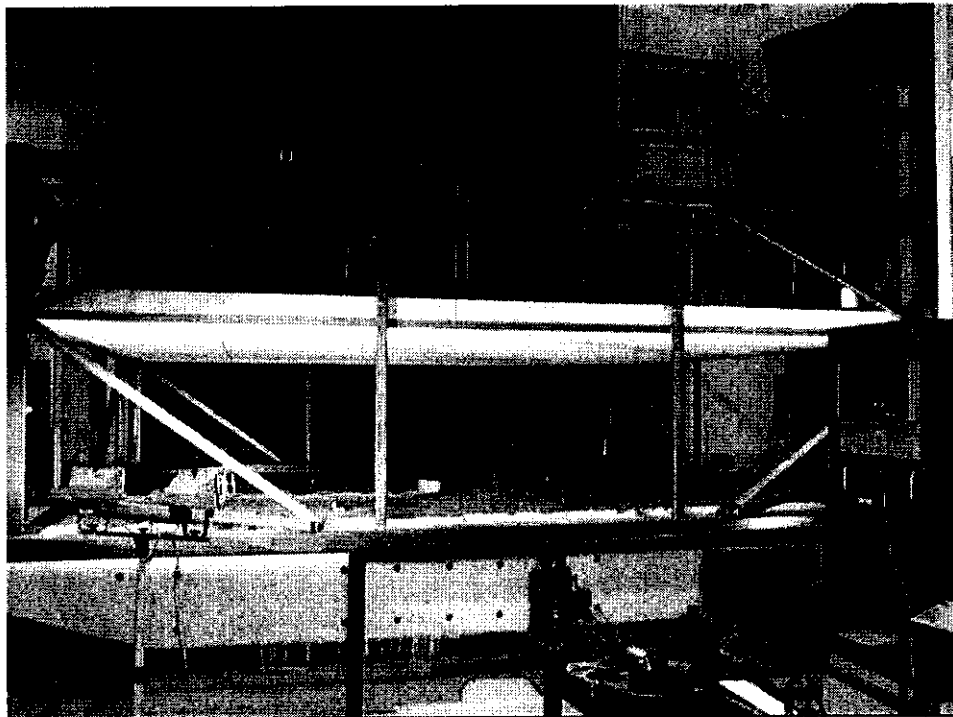
NIST developed a simple model to estimate the range of accelerations that might dislodge the SFRM from the structural steel components. As the SFRM in the towers was being upgraded with BLAZE-SHIELD II in the 1990s, The Port Authority had measured the insulation bond strength (force required to pull the insulation from the steel). The model used these data as input to some basic physics equations. The resulting ranges of accelerations depended on the geometry of the coated steel component and the SFRM thickness, density and bond strength. For a flat surface (as on the surface of a column), the range was from 20g to 530g, where g is the gravitational acceleration. For an encased bar (such as used in the WTC trusses), the range was from 40g to 730g. NIST estimated accelerations from the aircraft impacts of approximately 100g.

In determining the extent of insulation damage in each tower, NIST only assumed damage where dislodgement criteria could be established and supported through observations or analysis. Thus, NIST made the conservative assumption that insulation was removed only where direct debris impact occurred and did not include the possibility of insulation damage or dislodgement from structural vibration. This assumption produced a lower bound on the bared steel surface area, thereby making it more difficult to heat the steel to the point of failure.

6.9.4 Damage to Ceiling System

The aircraft impact modeling did not include the ceiling tile systems. To estimate whether the tiles would survive the aircraft impact, the University at Buffalo, under contract to NIST, conducted tests of WTC-like ceiling tile systems using their shake table (Figure 6–29) and impulses related to those induced by the aircraft impact on the towers. The data indicated that accelerations of approximately 5g would most likely result in substantial displacement of ceiling tiles. Given the estimated impact accelerations of approximately 100g, NIST assumed that the ceiling tiles in the impact and fire zones were fully dislodged. This was consistent with the multiple reports of severely damaged ceilings (Chapter 7).

An intact ceiling tile system could have provided the floor trusses with approximately 10 min to 15 min of thermal protection from ceiling air temperatures near 1,000 °C. These temperatures would quickly heat steel without thermal insulation to temperatures for reduction of the strength of structural steels.



Source: NIST

Figure 6–29. Ceiling tile system mounted on the shaking table.

6.9.5 Damage to Interior Walls and Furnishings

As shown in Figure 6–18, the aircraft impact simulations explicitly included the fracture of walls in the debris path and the “bulldozing” of furnishings. Damage to the impacted furnishings was not modeled. Walls and furnishings outside the debris paths were undamaged in the simulations.

6.10 THERMAL ENVIRONMENT MODELING

6.10.1 Need for Simulation

Following the impact of the aircraft, the jet-fuel-ignited fires created the sustained and elevated temperatures that heated the remaining building structure to the point of collapse initiation. The photographic evidence provided some information regarding the locations and spreading of the fires. However, the cameras could only see the periphery of the building interior. The steep viewing angles of nearly all of the photographs and videos further limited the depth of the building interior for which fire information could be obtained. NIST could not locate any photographic evidence regarding the fire exposure of the building core or the floor assemblies.

The simulations of the fires were the second computational step in the identification of the probable sequences leading to the collapse of the towers. The required output of these simulations was a set of three-dimensional, time varying renditions of the thermal and radiative environment to which the structural members in the towers were subjected from the time of aircraft impact until the onset of building collapse. The rigor of the Investigation placed certain requirements on the computational tool (model) used to generate these renditions:

- Resolution of the varying thermal environment across key dimensions, e.g., the truss space;
- Representation of the complex combustibles;
- Computation of flame spread across the large expanses of the WTC floors; and
- Confidence in the accuracy of the predictions.

6.10.2 Modeling Approach

The time frame of the Investigation and the above requirements led to the use of the Fire Dynamics Simulator (FDS). Under development at NIST since 1978, FDS was first publicly released in February 2000 and had been used worldwide on a wide variety of applications, ranging from sprinkler activation to residential and industrial fire reconstructions. However, it had never before been applied to spreading fires in a building with such large floor areas.

Figure 6-30 shows how FDS represented the eight modeled floors (92 through 99) of the undamaged WTC 1. A similar rendition was prepared for floors 78 through 83 of WTC 2. The layout of each floor was developed from architectural drawings and from the information described in Section 5.8. There was a wide range of confidence in the accuracy of these floor plans, varying from high (for the floors occupied by Marsh & McLennan in WTC 1, for which recent and detailed plans were obtained) to low (for most of the space in WTC 2 occupied by Fuji Bank, for which floor plans were not available).

The effects of the aircraft impact were derived from the simulations described in Section 6.8. The portions of walls and floors that were “broken” in those simulations were simply removed from the FDS models of the towers. The furnishings outside the aircraft-damaged regions were assumed to be unmoved and undamaged. The treatment of furnishings within the impact zone is discussed later in this section.

FDS represented the spaces in which the fires and their effluent were to be modeled as a grid of rectangular cells. These grids included the walls, floors, ceilings, and any other obstructions to the movement of air and fire. In the final simulations, the grid size was 0.5 m x 0.5 m x 0.4 m high (1.6 ft x 1.6 ft x 1.3 ft.). Each floor contained about 125,000 grid cells, and the nature of each cell was updated every 10 ms (100 times every second). The computations were performed using parallel processing, in which the fires on each floor were simulated on a different computer. At the end of each 10 ms update, the processors exchanged information and proceeded to the computations for the next time interval. Each simulation of 105 min of fires for WTC 1 took about a week on eight Xeon computers with a combined 16 GB of memory. The simulations for WTC 2, with fewer floors and 60 min of real time fires, took about half the time.

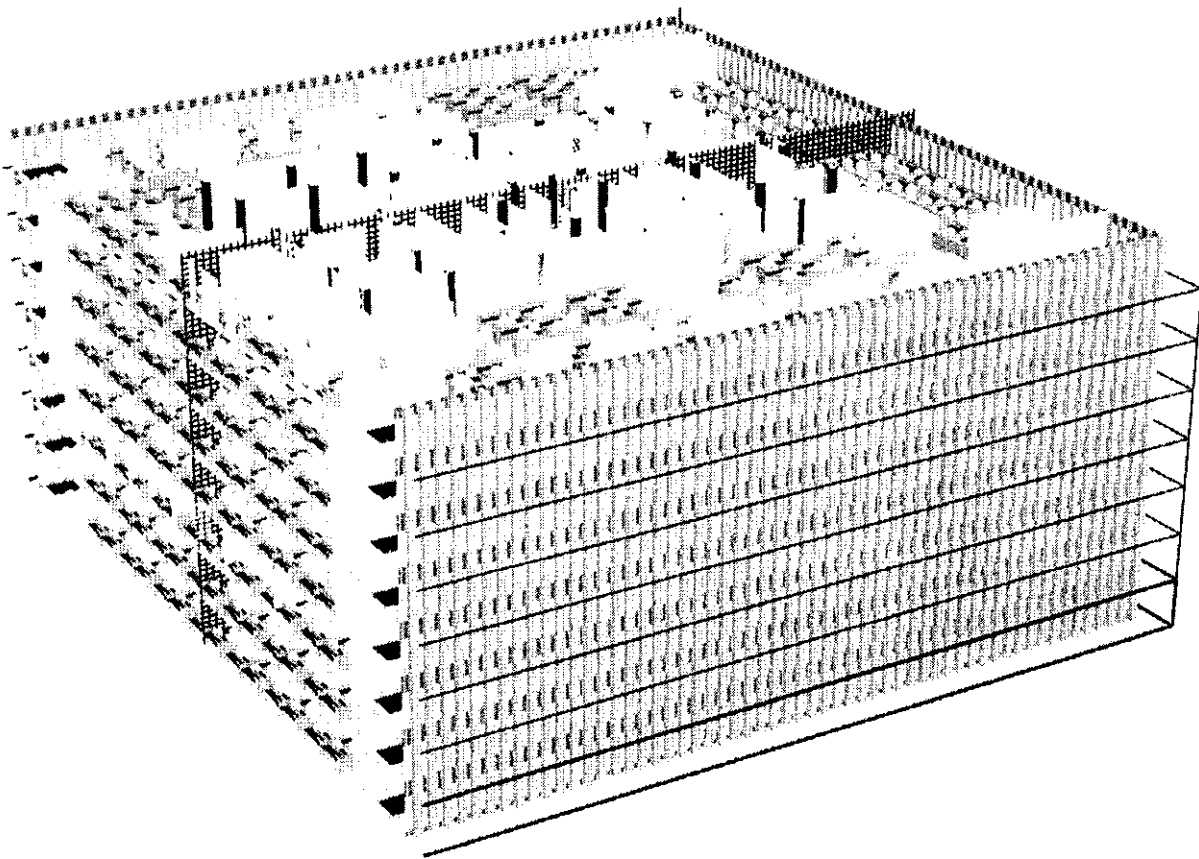
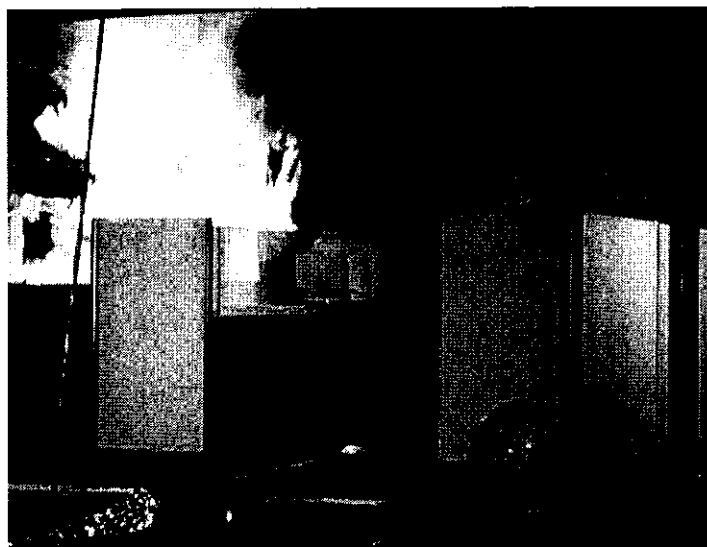


Figure 6–30. Eight floor model of WTC 1 prior to aircraft impact.

The fires were started by ignition of the jet fuel, whose distribution was provided by the aircraft impact simulations. The radiant energy from these short-lived fires heated the nearby combustibles, creating flammable vapors. When these mixed with air in the right proportion within a grid cell, FDS burned the mixture. This generated more energy, which heated the combustibles further, and continued the burning.

The floors of the tower on which the dominant burning occurred were characterized by large clusters of office workstations (Figure 1–11). NIST determined their combustion behavior from a series of single-workstation fire tests (Figure 6–31). In these highly instrumented tests, the effects of workstation type, the presence of jet fuel, and the presence of fallen inert material (such as pieces of ceiling tiles or gypsum board walls) on the burning surfaces were all assessed. While FDS properly captured the gross behavior of these fires, the state of modeling the combustion of real furnishings was still primitive. Thus, the results of this test series were used to refine the combustion module in FDS.



Source: NIST.

Figure 6–31. Fire test of a single workstation.

The accuracy of FDS predictions was then assessed using two different types of fire tests. In each case, the model predictions were generated prior to conducting the test.

The first series provided a measure of the ability of FDS to predict the thermal environment generated by a steady state fire. A spray burner generating 1.9 MW or 3.4 MW of power was ignited in a 23 ft by 11.8 ft by 12.5 ft high compartment. The temperatures near the ceiling approached 900 °C. FDS predicted:

The large fires discussed in this report are characterized by heat release rate, or burning intensity, (in MW), by total energy released (in GJ), and by the heat flux, or radiant intensity (in kW/m²).

- Room temperature increases near the ceiling to within 4 percent.
- Gas velocities at the air inlet to the compartment (and thus the air drawn into the compartment by the fire) within the uncertainty in the experimental measurements.
- The leaning of the fire plume due to the asymmetry of the objects within the compartment. The extent of the leaning was underestimated.
- Radiant heat flux near the ceiling to within 10 percent, within the uncertainty of the experimental measurements.

The second series was a preamble to the modeling of the actual WTC fires. Arrays of three WTC workstations were burned in a 35.5 ft by 23 ft by 11 ft high compartment (Figure 6–32). The tests examined the effects of the type of workstation, the presence of jet fuel, and the presence of fallen inert material on the burning surfaces. In one of the tests, the workstations were rubblized (Figure 6–33). Figure 6–34 depicts the intensity of the test fires. Figure 6–35 shows the measured and predicted heat release rate data from one of the tests in which there was no jet fuel nor inert material present.



Figure 6–32. Interior view of a three-workstation fire test.

Source: NIST.

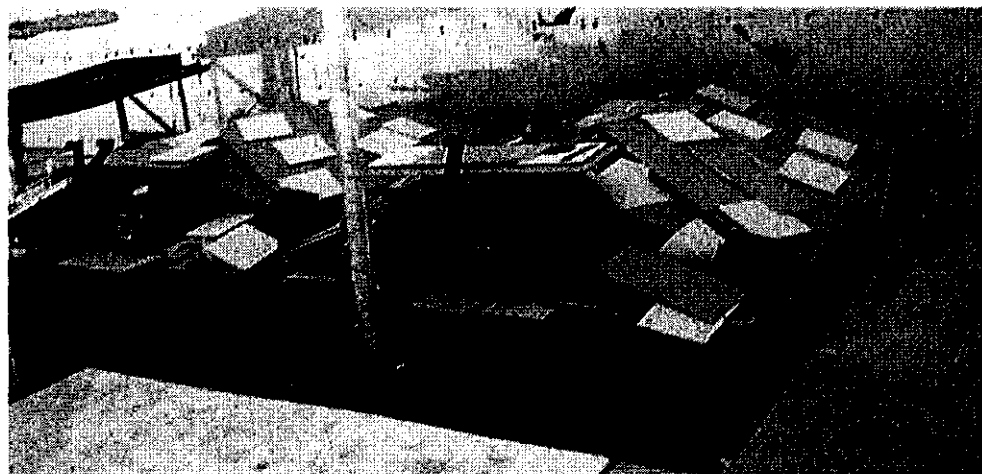
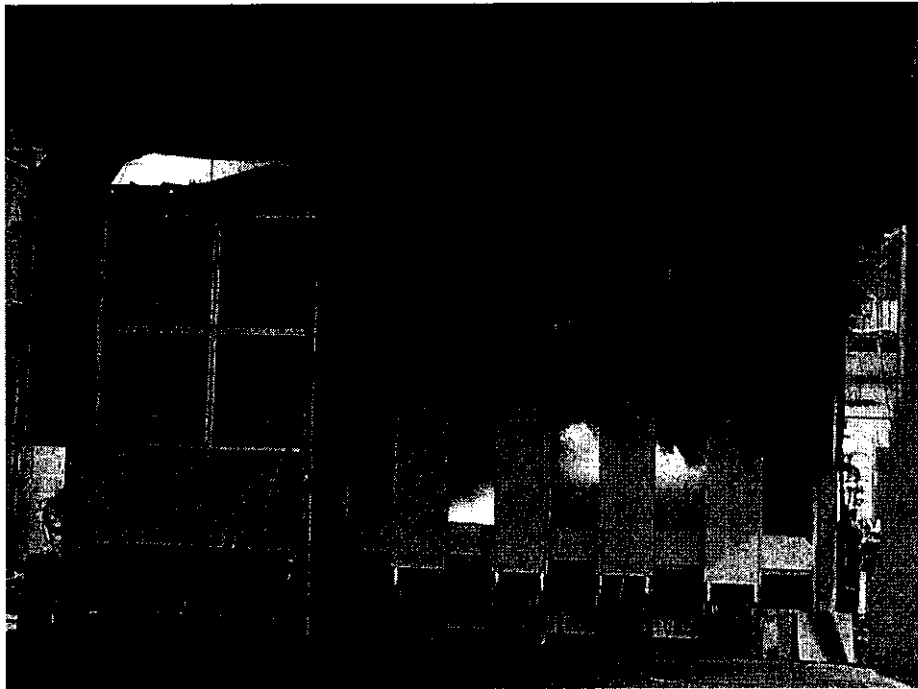


Figure 6–33. Rubblized workstations.

Source: NIST.



Source: NIST

Figure 6–34. Three-workstation fire test, 2 min after the start.

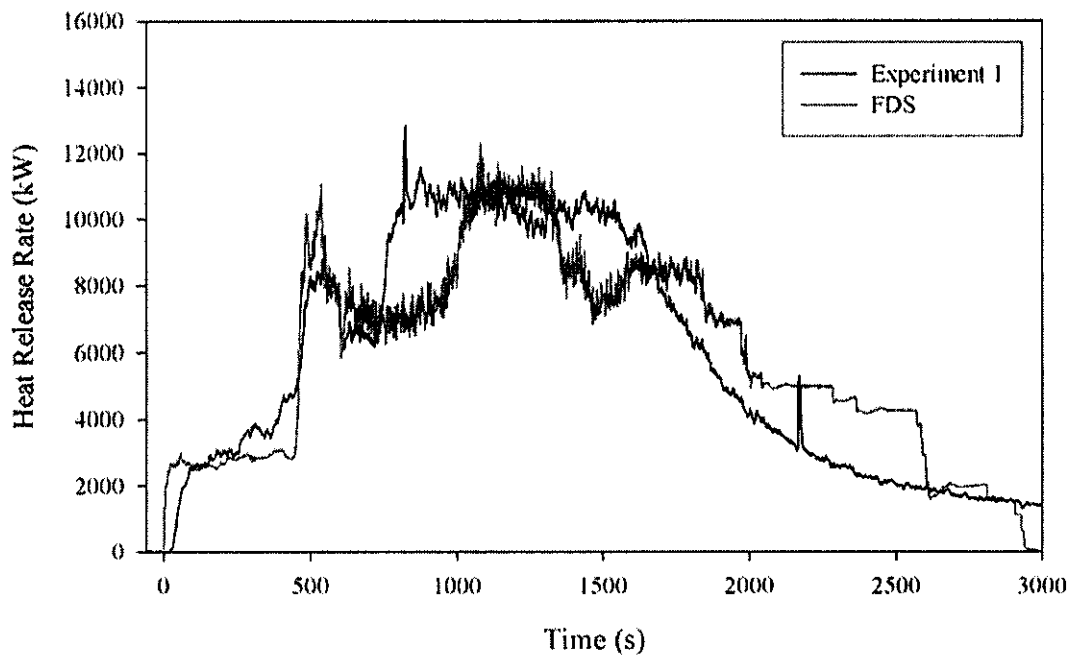


Figure 6–35. Measured and predicted heat release rate from the burning of three office workstations.

The differences in the fire behavior under the different experimental conditions were profound in these roughly hour-long tests. The jet fuel greatly accelerated the fire growth. Only about 60 percent of the

combustible mass of the rubblized workstations was consumed. The near-ceiling temperatures varied between 800 °C and 1,100 °C. Nonetheless, FDS successfully replicated:

- The general shape and magnitude of the time-dependent heat release rate.
- The time at which one half of the combustion energy was released to within 3 min.
- The value of the heat release rate at this time to within 9 percent.
- The duration of the fires to within 6 min.
- The peak near-ceiling temperature rise to within 10 percent.

All these predictions were within the combined uncertainty in the model input data and the experimental measurements.

Combined, these results led to the assessment that the uncertainty in the thermal environment predictions of the WTC fires would be dominated less by the FDS errors and more by the unknowns in such factors as the distribution of the combustibles, ventilation, and building damage.

6.10.3 The Four Cases

Four fire scenarios (Case A and Case B for WTC 1 and Case C and Case D for WTC 2) were superimposed on the four cases of aircraft-driven damage of the same names (Section 6.9).

A number of preliminary simulations had been performed to gain insight into the factors having the most influence on the severity of the fires. The most influential was the mass of combustibles per unit of floor area (fuel load); second was the extent of core wall damage, which affected the air supply for the fires. The aforementioned workstation fire tests had also indicated that the damage condition of the furnishings also played a key role. The scenario variables and their values are shown in Table 6–6.

Table 6–6. Values of WTC fire simulation variables.

Variable	WTC 1		WTC 2	
	Case A	Case B	Case C	Case D
Tenant combustible fuel load ^a	4 lb/ft ²	5 lb/ft ²	4 lb/ft ²	5 lb/ft ²
Distribution of disturbed combustibles	Even	Weighted toward the core	Heavily concentrated in the northeast corner	Moderately concentrated in the northeast corner
Condition of combustibles	Undamaged except in impact zone	Displaced furniture rubblized	All rubblized	Undamaged except in impact zone
Representation of impacted core walls ^b	Fully removed	Soffit remained	Fully removed	Soffit remained

a. In addition, approximately 27,000 lb of solid combustibles from the aircraft were distributed along the debris path.

b. In Cases A and C, the walls impacted by the debris field were fully removed. This enabled rapid venting of the upper layer into the core shafts and reduced the burning rate of combustibles in the tenant spaces. In Cases B and D, a more severe representation of the damage was to leave a 4 ft gypsum wallboard soffit that would maintain a hot upper layer on each fire floor. This produced a fire of longer duration near the core columns and the attached floor membranes.

FDS contained no algorithm for breaking windows from the heat of the fires. Thus, during each simulation, windows were removed at times when photographs indicated they were first missing. Damage to the ventilation shafts was derived from the aircraft impact simulations. For undamaged floors, all the openings to the core area were assumed to total about 50 ft² in area.

6.10.4 Characterization of the Fires

For each of the four scenarios, FDS was used to generate a time-dependent gas temperature and radiation environment on each of the floors. The results of the FDS simulations of the perimeter fire were compared with the fire duration and spread rate as seen in the photographs and videos. For ease of visualization, contour plots of the room gas temperature 1.3 ft below the ceiling slab (in the “upper layer” of the compartment) were superimposed on profiles of the photographed fire activity. An example is shown in Figure 6–36. The stripes surrounding the image represent a summary of the visual observations of the windows, with the black stripes denoting broken windows, the orange stripes denoting external flaming, and the yellow stripes denoting fires that were seen inside the building. Fires deeper than a few meters inside the building could not be seen because of the smoke obscuration and the steep viewing angle of nearly all the photographs.

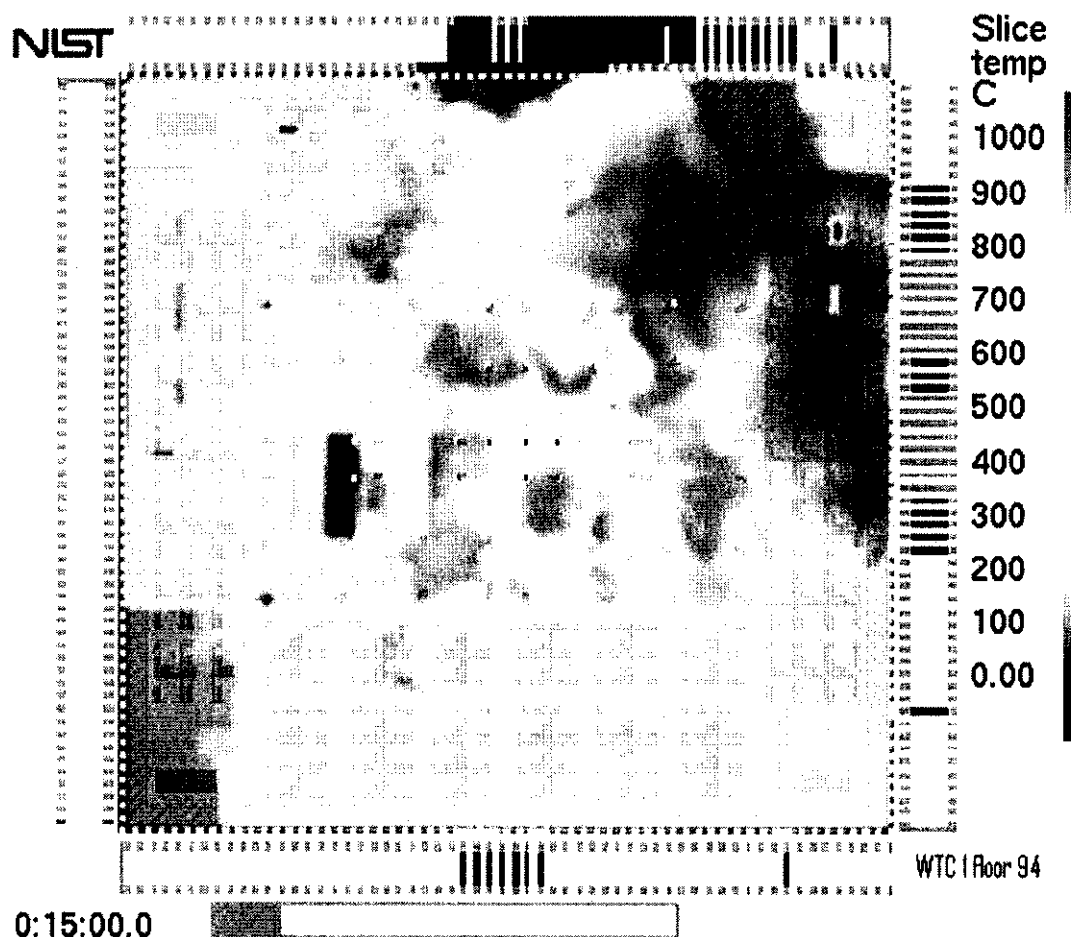


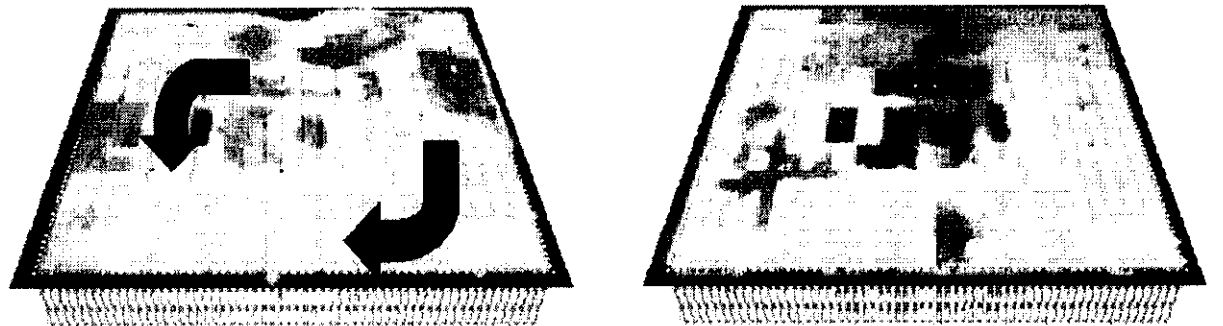
Figure 6–36. Upper layer temperatures on the 94th floor of WTC 1, 15 min after impact.

Given the uncertainties in some of the floor plans, the damage to the internal walls, and movement of the office furnishings, the intent of the simulations was to capture the magnitudes of the fires and the broad features of their locations and movement; and they did so.

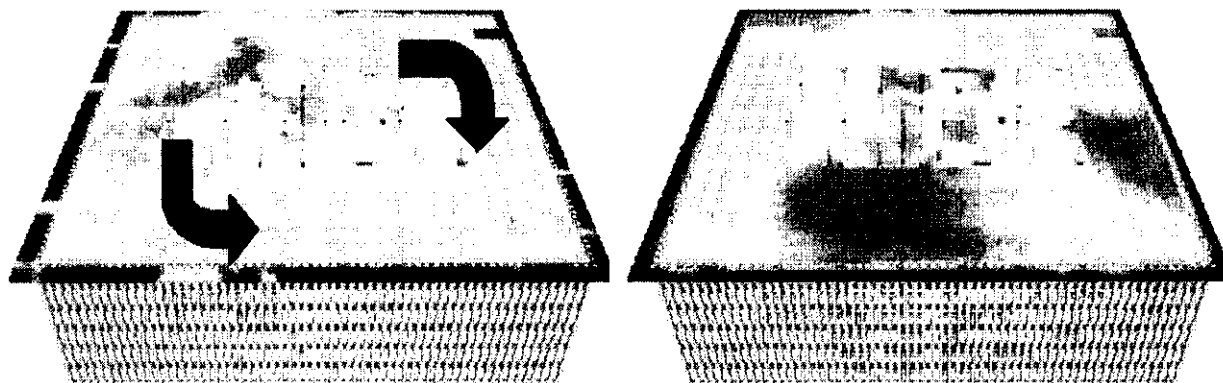
The following sections summarize the simulated behavior of the fires (which was used in the following stages of the disaster reconstruction) and their correlation with the analysis of the photographic evidence.

WTC 1

Much of the fire activity was initially in the vicinity of the impact area in the north part of the building. As a result of the orientation of the impacting aircraft and its fuel tanks, the early fires on the 92nd through 94th floors tended toward the east side of the north face, while the early fires on the 97th through 99th floors tended toward the west side of the north face. The fires on all the floors spread along the east and west sides and were concentrated in the south part of the building at the time of collapse, as depicted in Figure 6–37.



WTC 1, Floor 94



WTC 1, Floor 97

Figure 6–37. Direction of simulated fire movement on floors 94 and 97 of WTC 1.

The fire simulation results for Case A and Case B were similar, indicating only a modest sensitivity to the fuel load and the degree of aircraft-generated damage. This was because, in general, the size and movement of the fires in WTC 1 were limited by the supply of air from the exterior windows. Since the window breakage pattern was not changed in Case B, the additional and re-distributed combustibles within the building did not contribute to a *larger* fire. The added fuel did slow the spread slightly because the fires were sustained longer in any given location.

Although there was generally reasonable agreement between the simulated and observed fire spread rates, there were instances where the fires burned too quickly and too near the windows. This resulted from an artifact of the model: the combustible vapors burned immediately upon mixing with the incoming oxygen.

Simulations performed with doubled fuel loads slowed the fire spread well below the observed rates. Combined with the above results, this suggested that the estimated overall combustible load of 4 lb/ft² was reasonable.

The simulations showed high temperatures in some of the elevator shafts. The late fire observed on the west face of the 104th floor may have started from fuel gases in the core shafts that had accumulated over the course of the first hour of fires below. The presence of fire in the shafts on the 99th floor provided some support for this hypothesis, but no simulations were performed for floors higher than the 99th.

The predictions of maximum temperatures (e.g., red zones in Figure 6-37) were consistent with those in the three-workstation fire tests.

The use of an “average” gas temperature was not a satisfactory means of assessing the thermal environment on floors this large and would also have led to large errors in the subsequent thermal and structural analyses. The heat transferred to the structural components was largely by means of thermal radiation, whose intensity is proportional to the fourth power of the gas temperature. At any given location, the duration of temperatures near 1,000 °C was about 15 min to 20 min. The rest of the time, the calculated temperatures were near 500 °C or below. To put this in perspective, the radiative intensity onto a truss surrounded by smoke-laden gases at 1,000 °C was approximately 7 times the value for gases at 500 °C.

WTC 2

Simulating the fires in WTC 2 posed challenges in addition to those encountered in simulating the fires in WTC 1. The aircraft, hitting the tower to the east of center, splintered much of the furnishings on the east side of the building and plowed them toward the northeast corner. Neither the impact study nor the validation experiments performed at NIST could be completely relied upon to predict the final distribution, condition, and burning behavior of the demolished furnishings. In addition, only the layouts of the 78th and 80th floors were available to the Investigation; the other floors were only roughly described by former occupants. As a result of these unknowns, the uncertainty in these calculations was distinctly greater than in those for WTC 1. To help mitigate gross differences between the simulations and the observables, NIST made floor-specific adjustments, based on the results of preliminary computations. In particular, the fuel load and volatility on the 80th floor were reduced, and the fuel load on the 81st and 82nd floors was increased.

In contrast with WTC 1, in WTC 2 there was less movement of the fires. The major burning occurred along the east side, with some spread to the north. There was no significant burning on the west side of the tower.

Also unlike WTC 1, changing the combustible load in WTC 2 had a noticeable effect on the outcome of the simulations. Because so many windows on the impact floors in WTC 2 were broken out by the aircraft debris and the ensuing fireballs, there was an adequate supply of air for the fires. Thus, the burning rate of the fires was determined by the fuel supply. In the Case D simulation, the office furnishings and aircraft debris were spread out over a wider area, and the furnishings away from the impact area were undamaged. Both of these factors enabled a higher burning rate for the combustibles.

In general, the Case D simulations more closely approximated the observations in the photographs and videos, although there was still some prediction of burning too close to the perimeter, especially on the east side of the 78th, 79th, 81st and 83rd floors. The burning in the northeast corner of the 81st and 82nd floors was more intense in Case D than in Case C. The fire in the east side of the 79th floor burned more intensely and reached the south face sooner.

Nothing in the simulations explained the absence of fires in the “cold spot,” the 10-window expanse toward the east of the north face of the 80th, 81st, and 82nd floors.

6.10.5 Global Heat Release Rates

Much of the information needed to simulate the fires came from laboratory-scale tests. While some of these involved enclosures several meters in dimension and fires that reached heat release rates of 10 MW and 12 GJ in total heat output, they were still far smaller than the fires that burned in the WTC towers. Figure 6–38 shows the heat release rates from the FDS simulations of the WTC fires. The peak plateau heat release rates were about 2 GW for WTC 1 and 1 GW for WTC 2. Integrating the areas under these curves produced total heat outputs from the simulated fires of about 8,000 GJ from WTC 1 and 3,000 GJ from WTC 2.

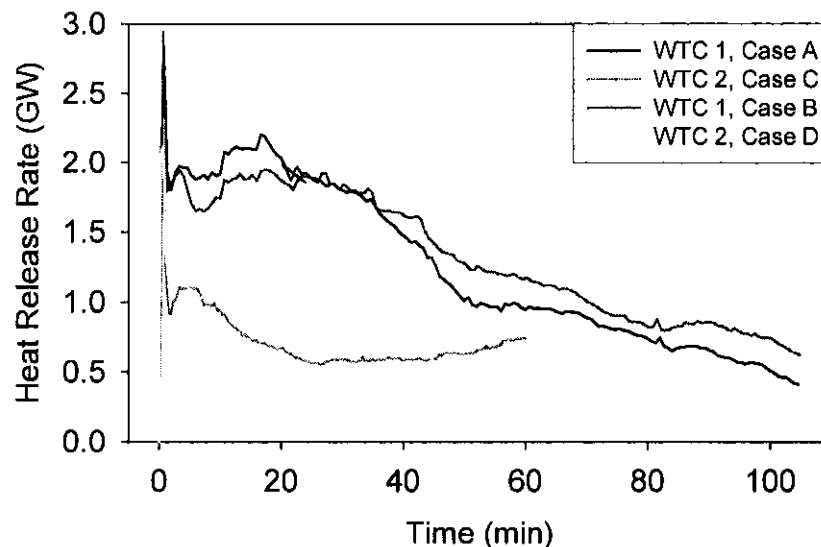


Figure 6–38. Predicted heat release rates for fires in WTC 1 and WTC 2.

6.11 DATA TRANSFER

The following data from FDS were compiled for use as boundary conditions for the finite-element calculation of the structural temperatures:

- The upper and lower layer gas temperatures, time-averaged over 100 s and spatially averaged over 3 ft. The upper layer gas temperatures were taken 1.3 ft (one grid cell) below the ceiling. The lower layer temperatures were taken 1.3 ft above the floor.
- The depth of the smoke layer.
- The absorption coefficient of the smoke layer 1.3 ft below the ceiling.

6.12 THERMAL MAPPING

6.12.1 Approach

Simulating the effect of a fire on the structural integrity of a building required a means for transferring the heat generated by the fire to the surfaces of the insulation on structural members and then conducting the heat through those members. In the Investigation, this meant mapping the time- and space-varying gas temperatures and radiation field generated by FDS onto and throughout the (insulated) columns, trusses and other elements that made up the tower structure.

This process was made difficult for these large, geometrically complex buildings by the wide disparity in length and time scales that had to be accounted for in the simulations. FDS generated thermal maps with dimensional resolution of the order of a meter and temperatures fluctuating on a time scale of milliseconds. The finite element models for thermal analysis resolved length of the order of $\frac{1}{2}$ in. on a time scale of seconds. Devising a computation scheme to accommodate the finest of these scales, while simulating the largest of these scales, presented a software challenge in order to avoid unacceptably long computation times.

6.12.2 The Fire-Structure Interface

NIST developed a computational scheme to overcome this difficulty, the Fire Structure Interface (FSI).

These computations began with the structural models of each WTC tower as described in Section 6.6.4, damaged by the aircraft as described in Section 6.8.4 and exposed to fire-generated heat, as described in Section 6.10.4. For a particular tower and damage scenario, FSI “bathed” each small section of each structural member in an air environment that had been generated by FDS. For efficiency of computation, two simplifications were made:

- The fluctuating environment was averaged over 30 s intervals, and

The transfer of radiant energy from a hot mass to a cool mass is proportional to the absolute temperature (Kelvin) to the fourth power. Thus, the contribution of the hot upper layer dominates the overall radiative heat transfer. Convective heat transfer is linearly proportional to the difference in temperature between the hot gas and the cool solid.

- The local environment was represented by a hot, soot-laden upper layer and a cooler, relatively clear lower layer.

FSI then calculated the radiative and convective heat transfer to each of these small sections using conventional physics. Finally, the temperature data were read into the ANSYS 8.0 finite element program, which applied the temperature distribution to the structural elements.

6.12.3 Thermal Insulation Properties

Equivalent Uniform Thickness of SFRM

Preliminary simulations with FSI explored the extent to which bare steel structural elements would heat more rapidly than the same elements would if they were well insulated. In one such calculation experiment, one of the largest columns in the tower structure was immersed in a furnace at 1,100 °C. Uninsulated, it took just 13 min for the steel surface temperatures to reach 600 °C, in the range where substantial loss of strength occurs. When insulated with 1 1/8 in. of SFRM, the same column had not reached that temperature in 10 hours. This established that the fires in WTC 1 and WTC 2 would not be able to significantly weaken the insulated core or perimeter columns within the 102 min and 56 min, respectively, after impact and prior to collapse. Thus, it was important to know whether the insulation was present or removed and much less important to know the exact thickness of the SFRM.

It was likely that the thinner steel bars and angles in the floor trusses would be more sensitive to the condition of the insulation. If the insulation were present, but too thin or imperfectly applied, these components might have been heated to failure in times on the order of an hour.

NIST performed additional simulations to probe the effect of gaps in the truss insulation and of variations in the thickness, similar to those observed in real SFRM application (Figure 5–6). It was evident that incorporation of these small-scale variations into the description of the structural members would have lengthened the FSI computations to an extreme. Furthermore, there was insufficient information to determine how the thickness varied over the length of the structural members. NIST combined the measured variations in the SFRM thickness (as described in Section 5.6.2) with simulations of the heat transfer through the uneven material. This led to the identification of a uniform thickness that provided the same insulation value as did the measured coatings. These values, shown in Table 5–3, were used in the thermal calculations. They were found to be greater than the specified thicknesses but slightly smaller than the average measured thicknesses, as they should be.

SFRM Thermophysical Properties

When the Investigation began, there were few published data on the insulating properties of SFRMs, especially at elevated temperatures. It was expected, and soon confirmed, that the fires could generate temperatures up to 1,100 °C. Therefore, NIST contracted for measurement of the key SFRM thermophysical properties that, along with coating thickness, determine the insulating effect of the coatings. These properties included thermal conductivity, specific heat capacity, and density. These were measured for each SFRM at temperatures up to 1,200 °C. Since there were no ASTM test methods developed specifically for characterizing the thermophysical properties of SFRMs as a function of temperature, ASTM test methods developed for other materials were used. Samples were prepared by the

manufacturers of the fire-resistive material, which included BLAZE-SHIELD DC/F and BLAZE-SHIELD II.

- The thermal conductivity measurements were performed according to ASTM C 1113, Standard Test Method for Thermal Conductivity of Refractories by Hot Wire (Platinum Resistance Thermometer Technique). The room temperature values were in general agreement with the manufacturer's published values for both materials. The thermal conductivities increased with temperature.
- Specific heat capacity was measured in accordance with ASTM E 1269, Standard Test Method for Determining Specific Heat Capacity by Differential Scanning Calorimetry (DSC). By including DSC measurement of a NIST Reference Material (sapphire), the measured SFRM quantities were directly traceable to NIST standards.
- The densities of the SFRMs were calculated from measurements of changes in the mass and dimensions of samples as their temperatures were increased. The length-change measurements were performed according to ASTM E 228, Standard Test Method for Linear Thermal Expansion of Solid Materials. The mass loss measurements were performed according to ASTM E 1131, Standard Test Method for Compositional Analysis by Thermogravimetry.

It was not known which type(s) of gypsum wallboard were used to enclose the core columns. Therefore, the thermophysical properties of four types of gypsum panels were examined.

- Thermal conductivity was measured using the heated probe technique described in ASTM D 5334, Standard Test Method for Determination of Thermal Conductivity of Soil and Soft Rock by Thermal Needle Probe Procedure. In general, the thermal conductivity initially decreased as the temperature increased to 200 °C and then increased with increasing temperature above 300 °C.
- Specific heat capacities of the cores of the four gypsum panel samples were measured using a differential scanning calorimeter at NIST according to ASTM E 1269, Standard Test Method for Determining Specific Heat Capacity by Differential Scanning Calorimetry. The four panels had nearly identical specific heat capacities as a function of temperature.
- The variation of density with temperature was determined from the change in volume of the gypsum material and the mass loss. The linear expansion was determined using a dilatometer and the mass loss from thermogravimetric analysis. All four materials showed the same trend as a function of temperature.

6.12.4 FSI Uncertainty Assessment

As was done for FDS, it was necessary to establish the quality of FSI's predictions of temperature profiles within insulated and bare structural steel components. This was accomplished using data from a series of six tests in which assorted steel members were exposed to controlled fires of varying heat release rate and radiative intensity. The steel members, depicted in Figures 6-39 through 6-41, were either bare or coated with sprayed BLAZE-SHIELD DC/F in two thicknesses. The fibrous insulation was applied by an

experienced applicator, who took considerable care to apply an even coating of the specified thickness. As such, the insulated test subjects represent a best case in terms of thickness and uniformity. Figure 6-42 shows some of the coated components.

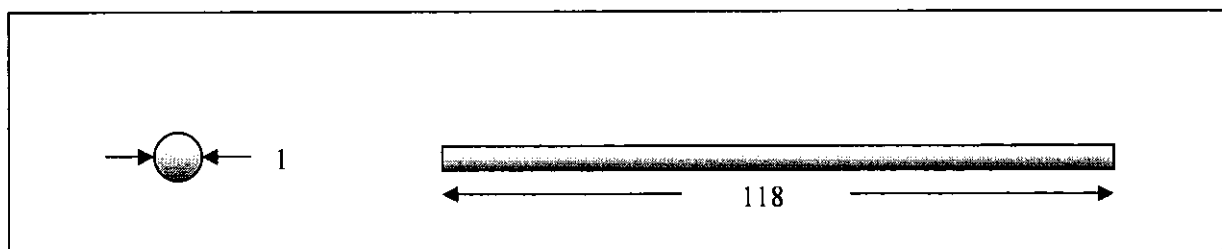


Figure 6-39. Simple bar dimensions (in.).

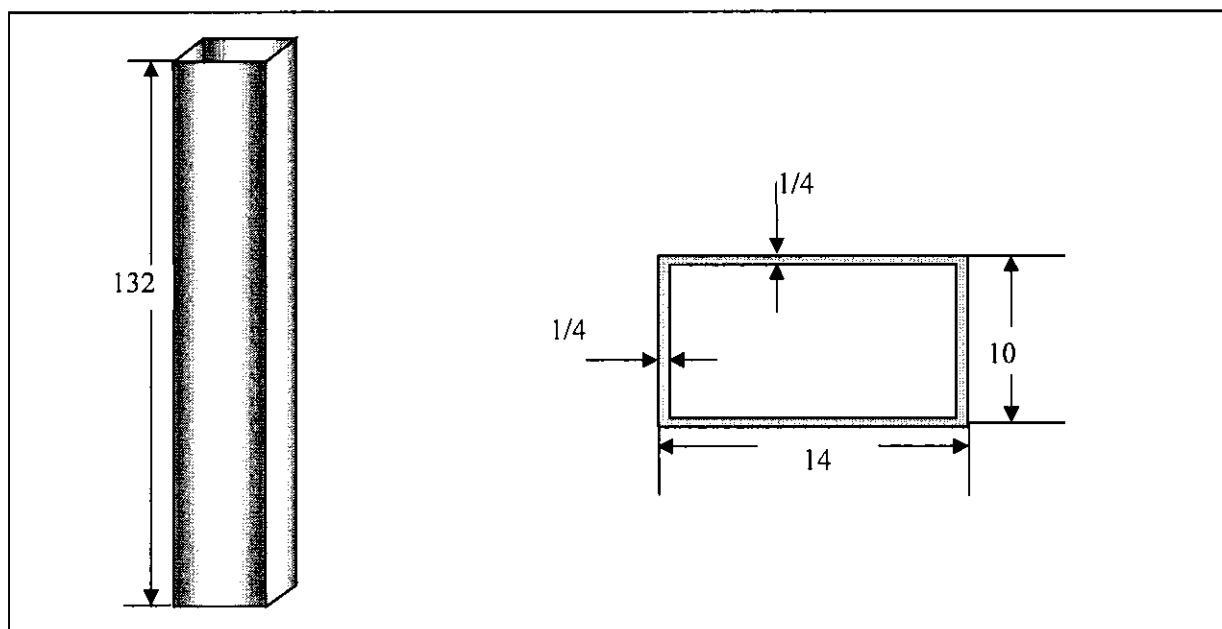


Figure 6-40. Tubular column dimensions (in.).

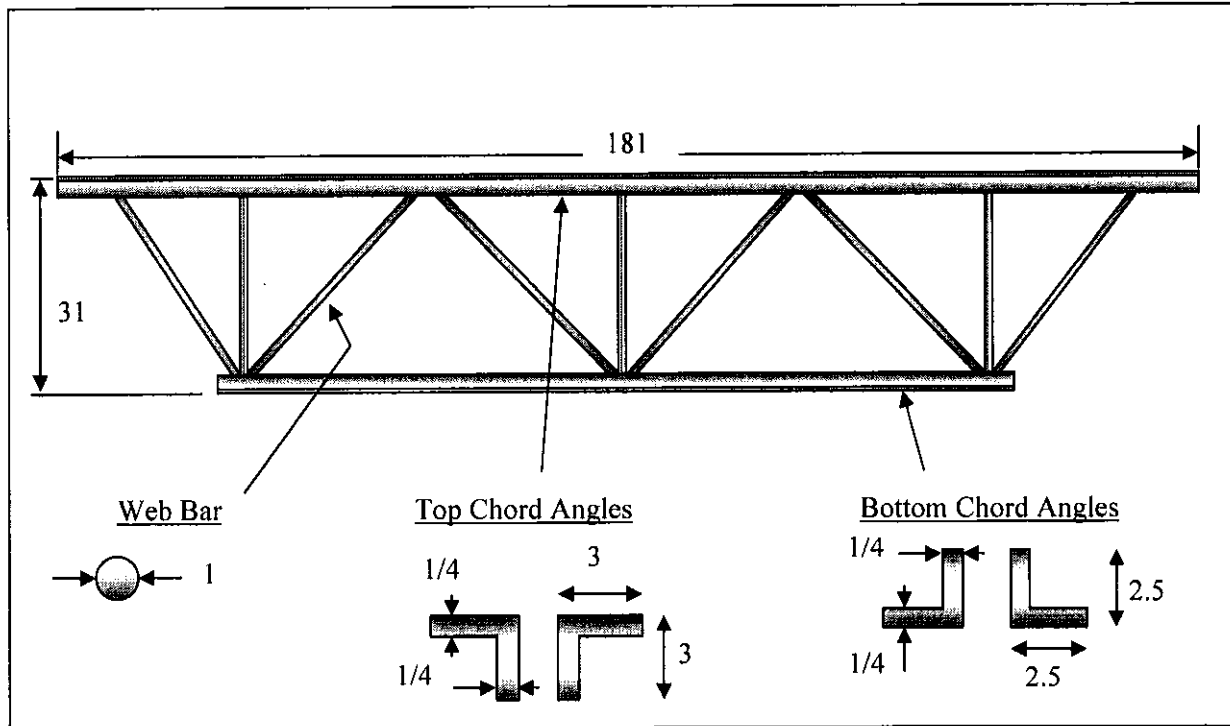


Figure 6-41. Truss Dimensions (in.).



Source: NIST.

Figure 6-42. SFRM-coated steel components prior to a test.